The ultrasonic vibration-assisted polishing material removal model of tilted cylindrical polishing tool based on BK7 glass

Zhijie Cui (bonnenuit_c@163.com)
Northeastern University School of Mechanical Engineering and Automation
Yingdong Liang
Xin Chen
Fanwei Meng
Zixuan Wang
Tianbiao Yu
https://orcid.org/0000-0002-6161-8838
Ji Zhao

Research Article

Keywords: ultrasonic vibration-assisted polishing, material removal model, maximum removal depth, material removal rate

Posted Date: August 10th, 2022

DOI: https://doi.org/10.21203/rs.3.rs-1915644/v1

The ultrasonic vibration-assisted polishing material removal model of tilted cylindrical polishing tool based on BK7 glass

Zhijie Cui [a, b], Yingdong Liang [a, b], Xin Chen [a, b], Fanwei Meng [a, b], Zixuan Wang [a, b], Tianbiao Yu [a, b, *], Ji Zhao [a, b, **]

[a] School of Mechanical Engineering and Automation, Northeastern University, Shenyang, 110819, PR China

[b] Liaoning Provincial Key Laboratory of High-end Equipment Intelligent Design and Manufacturing Technology, Northeastern University, Shenyang, 110819, PR China

* Corresponding author. Northeastern University, Shenyang, 110819, PR China

** Corresponding author. Northeastern University, Shenyang, 110819, PR China

Author	E-mail
Zhijie Cui	bonnenuit_c@163.com
Yingdong Liang	1910112@stu.neu.edu.cn
Xin Chen	northeastern_cx@163.com
Fanwei Meng	mengfanwei6699@163.com
Zixuan Wang	wangzx@mail.neu.edu.cn
Tianbiao Yu	tianbiaoyudyx@gmail.com
Ji Zhao	jzhao@mail.neu.edu.cn

Abstract:

BK7 glass is widely used in various optical instruments as common ceramic material. However, there are still several difficulties in the polishing process due to its material properties. Ultrasonic vibration-assisted polishing (UVAP) is used widely for its excellent material removal properties. However, there are few researches on the model of UVAP material removal for tilted. Therefore, this paper investigates this problem. A model of UVAP material removal was established for titled column polishing; The pressure distribution and velocity distribution in the contact zone were modeled by means of experiments and geometric analysis. A series of orthogonal experiments were conducted, and the experimental results showed that the coefficient of determination was above 0.9 after fitting the actual profile to the predicted profile. The results of the orthogonal experiments were also analyzed by ANOVA. The predict error of maximum removal depth was less than 13.12%. The error of material removal rate (MRR) was less than 9.24%. By PSD analysis, it was found that the introduction of ultrasonic amplitude has a good effect on suppressing the medium and high frequency errors on the machined surface. The novel model can be used to optimize machining parameters and provide theoretical support for complex parts polishing.

Keywords: ultrasonic vibration-assisted polishing; material removal model; maximum removal depth; material removal rate

1. Introduction

As science and technology improve by leaps and bounds, more and more precision instruments are put into daily use. Hard and brittle materials [1–4] are widely used in these instruments for their wear resistance, corrosion resistance and excellent mechanical properties. The processing methods of hard and brittle materials have also been studied by scholars [5, 6]. BK7 is widely used as a general optical glass in the optical systems [7–9]. However, due to the influence of material properties, BK7 glass encounters many problems during processing [10]. Traditional machining methods such as grinding and polishing are difficult to avoid problems such as low machining efficiency [11], while ultrasonic vibration-assisted machining has many advantages in increasing machining efficiency and improving machined surface quality. Ultrasonic-assisted grinding of BK7 glass has been studied by many scholars internationally [12, 13], and process optimization has been performed in grinding force, grinding thickness, and grinding temperature [14–17]. As a ultra-precision machining method, polishing is an important method to achieve nano-scale machining. Many scholars have also conducted various studies on polishing methods [18–20]. Due to the little research on the mechanism of UVAP of BK7 glass, the method is not widely used in actual processing. Compared with traditional polishing methods, UVAP can significantly improve the polishing efficiency, so it is essential to conduct an intensive study on the polishing mechanism of UVAP.

Many researchers have investigated polishing equipment and theoretical models for UVAP. Zhang et al. [21] introduced the micromorphology of polishing tools during the study the polishing forces of UVAP. A model of the microscopic contact state during

UVAP was developed. The accuracy of the predicted model was verified experimentally, which is a guide for UVAP processing of brittle materials. Liang et al. [22] introduced an ultrasonic atomization device in UVAP. Taking BK7 optical glass as an example, the material removal mechanism of UVAP was analyzed and a material removal model was developed. Kang et al. [23] investigated ultrasonic vibration-assisted laser polishing (UVLP). A methodology for laser polishing through a lens driven by piezoelectric ceramics was proposed. The method of the theoretical analysis was verified by the comparison experiments of TLP and UVLP. The processing parameters of UVLP of 304 stainless steel were analyzed. Qu et al. [24] developed a material removal model for tilted-axis UVAP with a spherical polishing tool. The correctness of the predicted model was verified by comparing the material removal depth, MRP, and MRR. Moreover, the experimental results show that larger ultrasonic amplitude and tilt angle can effectively improve the material removal.

In addition to the above processing parameters, polishing tools have a significant impact on UVAP. Xiao et al. [25] investigated the polishing force for small inclination machining of circular polishing discs. The relationship between polishing force and contact depth, inclination angle, polishing disc, and workpiece radius of curvature was established. The model was validated by finite element simulations and experiments. This study provides a theoretical basis for achieving uniform material removal. Wang et al. [26] analyzed the material removal model after machining tilting polished discs. A material removal map was generated based on this removal model, and its correctness was verified by experiments. This study is essential for the selection and optimization

of processing parameters. Zhang et al. [27] proposed a surface profile model for UVAP by using a cylindrical polishing tool. The study introduced the concept of the Preston correction factor. It was found that the prediction results were consistent with the experimental results, which is an important guideline for the adjustment and selection of polishing parameters. Feng et al. [28] developed a corresponding material removal model for a tilted elastic polishing disc. The step size between polishing paths was investigated based on the model. The correctness of the model was verified by experiments.

In previous studies, there have been sufficient theoretical studies on material removal models for tilted column polishing tools, but few studied the effect of ultrasonic on it. Predictions of the surface profile of the UVAP formed by the straight feed of the column polishing head have been presented, but little research has been conducted on the material removal characteristics of UVAP of the tilted cylindrical polishing tool. This paper attempts to fill this gap.

2. The model of material removal

The polishing tool can deform considerably due to the polishing force when the spherical polishing tool was performed. And this deformation can have an impact on the accuracy of the material removal model. However, cylindrical polishing tools have less deformation and greater contact zone for the same processing parameters. Linear trajectory is performed as the common trajectory. In this paper, the model of UVAP material removal for tilted column polishing tools was investigated.

The contact diagram between the workpiece and the polishing tool is shown in Fig. 1. The polishing tool with radius R is mounted on the spindle of the polishing, point O is the critical point between the deformed and undeformed areas of the polishing tool. The feed direction is identical to the positive direction of the x-axis. α is the angle between the column polishing tool and the workpiece. The dashed part is the compression area of the polishing tool, whose depth h is defined as the displacement of the polishing tool along the normal of the workpiece surface. The spindle applies ultrasonic vibration of frequency f to the polishing tool.

In the process of polishing, the function of material removal is usually described by the Preston equation, which is given as:

$$\frac{dh(x,y)}{dt} = kv(x,y)p(x,y) \tag{1}$$

Where the material removal depth is denoted by $dh(x,y)$; the relative speed between the workpiece and the polishing tool is denoted by $v(x,y)$; and the polishing pressure is denoted by $p(x,y)$; k is the Preston coefficient, the value of k needs to be determined experimentally.

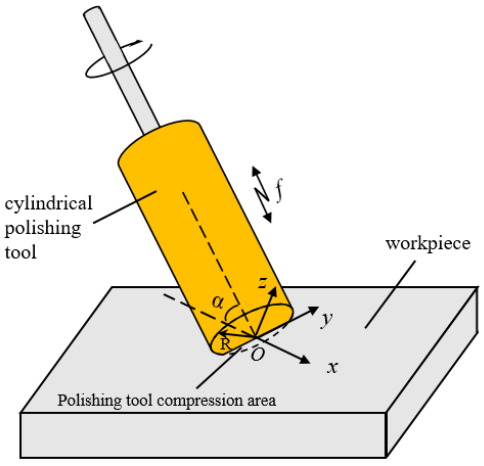

Fig. 1 Polishing tool contact schematic

2.1 Polishing pressure distribution model

As shown in Fig. 2, during the plane polishing process, when the compression of the polishing tool is E, the graphics enclosed by the line CB and the arc BGC can be represented as the polished contact zone. Where CB denotes the contact zone width $2W$ and OG denotes the contact zone length L, the geometric relationship gives:

$$L = \frac{E^{'}}{\sin\theta} \tag{2}$$

$$W = \sqrt{R^2 - (R - L)^2} \tag{3}$$

When ultrasonic vibration is introduced, E' can be expressed as:

$$E^{'} = E + A\sin(2\pi ft + \varphi) \tag{4}$$

Where A and f are the ultrasonic amplitude and ultrasonic frequency; φ is the initial phase of ultrasonic vibration, in this study $\varphi = 0$. Substituting Eq. (4) into Eq. (2):

$$L = \frac{E + A\sin(2\pi ft + \varphi)}{\sin\theta} \tag{5}$$

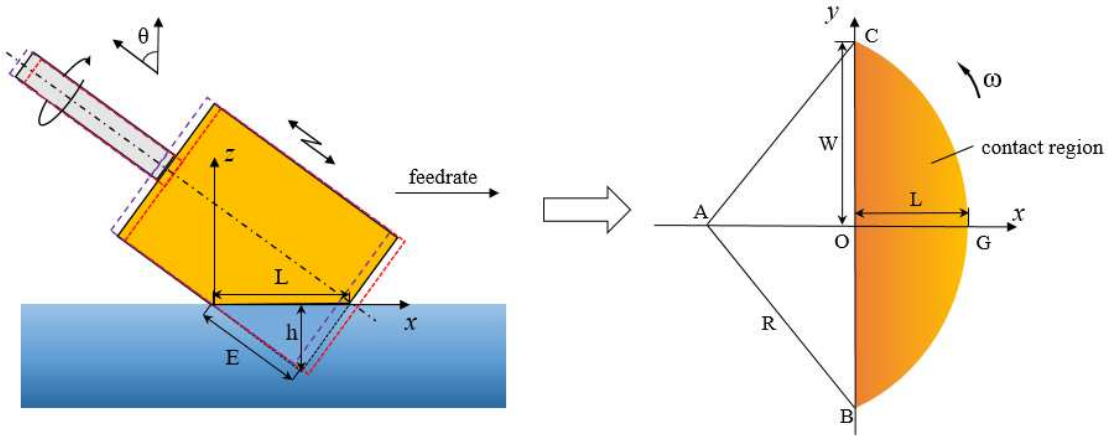

Fig. 2 Schematic diagram of contact zone

Due to the specificity of the contact zone in this paper, the Hertzian contact theory does not apply to this model. In this paper, the pressure distribution in the contact zone is analyzed by Feng's method [28]. Assume that the contact pressure at any position within the contact zone is directly proportional to the deformation variable, the specific

relationship is as follows:

$$p(x, y) = K \times e(x, y) \tag{6}$$

K is a constant that needs to be calculated by subsequent experiments. Considering the characteristics of ultrasonic vibrations, the pressure at any point in the contact zone can be expressed as:

$$p(t) = K \times \left[\frac{x}{\tan\theta} + \frac{A\sin(2\pi ft + \varphi)}{\cos\theta} \right] \tag{7}$$

In the modeling of polishing pressure distribution, the relationship between polishing pressure and compression needs to be analyzed first. This process is mainly realized by polishing force experiments. The polishing force is measured by a dynamometer (Kistler 9257B). The experiment chose 8 mm diameter column polishing tool, the inclination angle was set to 5°, 10°, 15° and 20° respectively, and the uniform compression amount was taken each time. The compression and polishing force curves are shown in Fig. 3. When the inclination angle is 5° and the ultrasonic amplitude is 0, the force-compression expression is:

$$F = -44.25x^3 + 54.14x^2 + 20.77x + 0.4285 \tag{8}$$

According to the polishing force equation:

$$F = \iint_S p(x, y)dS = \int_{-y}^{y} dy \int_0^{f(y)} p(x, y)dx \tag{9}$$

The value of the coefficient K can be calculated from different angles.

$$K = \frac{F\cos\theta}{\int_{-y'}^{y'} (\frac{1}{2} f(y)^2 g\sin\theta + A\sin(2\pi ft + \varphi) f(y))dy} \tag{10}$$

Where y' is the longitudinal coordinate of point C in Fig. 2, $y' = \sqrt{R^2 - (R-L)^2}$; *f(y)* represents the arc BCG, and $f(y) = \sqrt{R^2 - y^2} - R + L$.

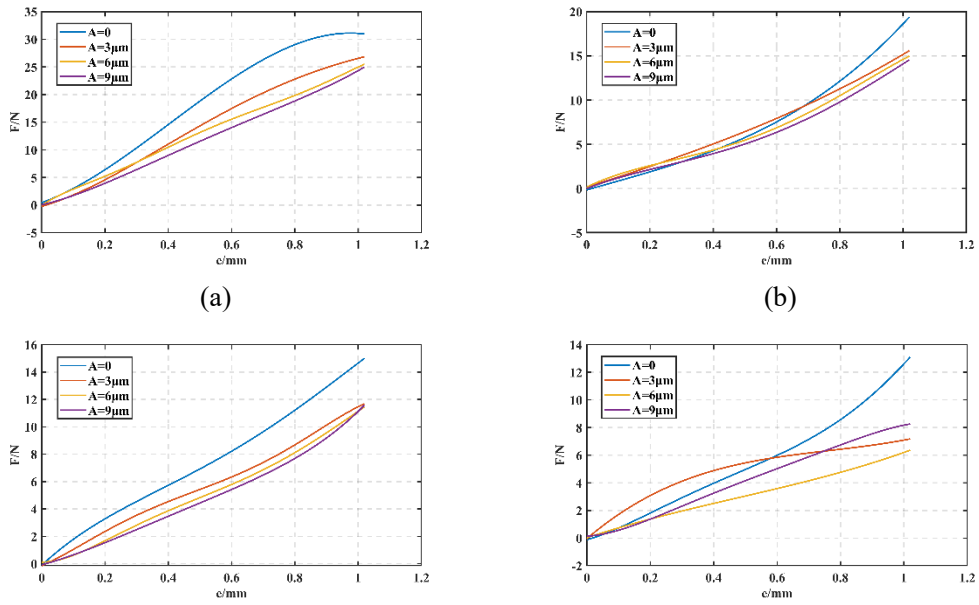

Fig. 3 Compression-force relationship curves: (a) polishing tool inclination of 5° (b) polishing tool inclination of 10° (c) polishing tool inclination of 15° (d) polishing tool inclination of 20°

When the polishing tool makes a linear feed motion on the workpiece, take a point *P* on the workpiece as an example. As shown in Fig. 4, position 1 is the polished contact zone just touching point *P*, which is the critical position for point *P* to produce material removal. When the polishing tool moves to position 2, point *P* is completely within the polishing area. Position 3 indicates that the polished contact zone is completely leaving point *P*. As shown in Fig. 5, to analyze the distribution of polishing pressure, the coordinate system *x*-*o*-*y* is established. The coordinate of point P1 is (*L*, *y*), and the coordinates of point P2 is $(\sqrt{R^2-y^2}-(R-L), y)$, when the polishing tool feed speed is v_f:

$$\begin{cases} t_1 = \dfrac{2L-\sqrt{R^2-y^2}-R}{v_f} \\ t_2 = \dfrac{\sqrt{R^2-y^2}-(R-L)}{v_f} \end{cases} \tag{11}$$

When point *P* moves between P1 and P2, it is not subjected to pressure. The

pressure distribution in the stage from P2 to P3 is shown in Eq. (7). When the polishing tool moves from P1 to P3, the polishing pressure can be indicated as:

$$p(x,y)=\begin{cases}0 & 0<t\le t_1\\ K\times\left[x\tan\theta+A\sin(2\pi ft+\varphi)\cos\theta\right] & t_1<t\le t_2\end{cases} \tag{12}$$

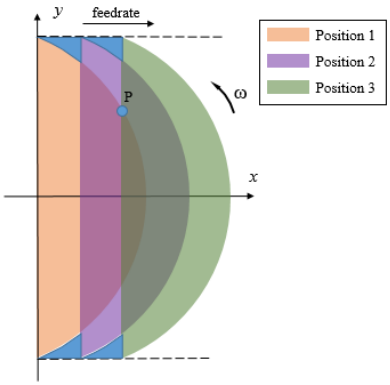

Fig. 4 Diagram of contact zone

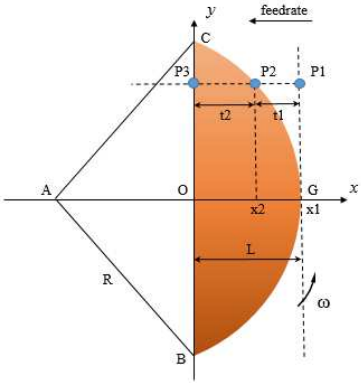

Fig. 5 Straight path polishing pressure distribution

2.2 Polishing area linear velocity distribution model

When the feed speed of polishing tool is 0, the velocity at any point of the polished area can be denoted:

$$v_s=\omega\sqrt{x^2+\left(R_t-L-y\right)^2} \tag{13}$$

The angular velocity of the spindle can be expressed as ω. The velocity distribution function in the polished contact zone can be represented by the linear velocity v_s of the polishing tool and the feed velocity v_f along the trajectory direction:

$$v_r=\sqrt{v_s^{\,2}+v_f^{\,2}+2v_sv_f\cos\theta} \tag{14}$$

Where, θ is the angle between v_s and v_f, and $0<\theta<\pi$. Fig. 6 shows a schematic diagram of the velocity along a straight line polished when the contact point is located in the positive direction of the y-axis.

$$\cos\theta=-\cos\left(\pi-\theta\right)=-\frac{y}{\sqrt{x^2+y^2}} \tag{15}$$

When the contact point is in the negative direction of the *y*-axis:

$$\cos\theta = -\frac{y}{\sqrt{x^2+y^2}} \tag{16}$$

Combined with Eqs. (13) - (16), the linear velocity distribution function in the contact zone can be represented:

$$v_r = \sqrt{\omega^2\left[y^2+\left(R_t-L-x\right)^2\right]+{v_f}^2+2\omega\sqrt{y^2+\left(R_t-L-x\right)^2}\cdot v_f\cdot\frac{y}{\sqrt{x^2+y^2}}} \tag{17}$$

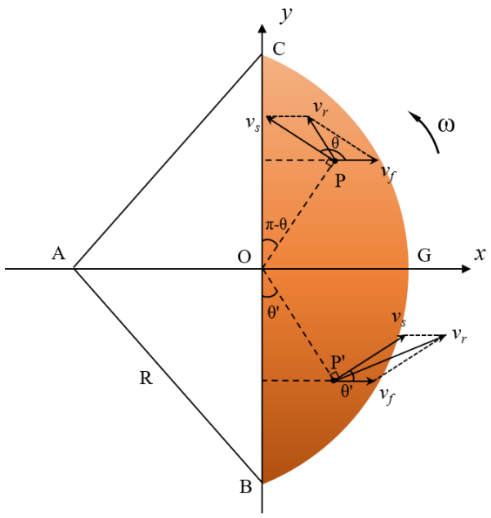

Fig. 6 Polishing area speed distribution

2.3 Material removal modeling

According to Eq. (7), the effect of ultrasonic vibration working time *t* was considered in this model. Combined with Eq. (1), the MRP at any point in the polished area can be written as a function of the ultrasonic vibration working time *t*:

$$dh(x,y) = k\cdot\left\{K\times\left[\frac{x}{\tan\theta}+\frac{A\sin(2\pi ft+\varphi)}{\cos\theta}\right]\right\}\sqrt{\omega^2\left[y^2+\left(R_t-L-x\right)^2\right]+{v_f}^2+2\omega\sqrt{y^2+\left(R_t-L-x\right)^2}\cdot v_f\cdot\frac{y}{\sqrt{x^2+y^2}}}dt \tag{18}$$

Assume that the distance of polishing tool movement in *dt* time is *dl*, then:

$$d_t = \frac{d_l}{v_f} \tag{19}$$

According to Fig. 4, for any point in the polishing area, the relationship between

the working time *dt* of ultrasonic vibration and the feed rate v_f can be expressed as:

$$t = \frac{x}{v_f} \tag{20}$$

Substituting Eqs. (19) and (20) into Eq (18):

$$dh(x,y) = \frac{k}{v_f} \cdot \left\{ K \times \left[\frac{x}{\tan\theta} + \frac{A\sin(2\pi f \frac{x}{v_f} + \varphi)}{\cos\theta} \right] \right\} \sqrt{\omega^2 \left[y^2 + \left(R_t - L - x \right)^2 \right] + v_f{}^2 + 2\omega \sqrt{y^2 + \left(R_t - L - x \right)^2} \cdot v_f \cdot \frac{y}{\sqrt{x^2 + y^2}}} dl \tag{21}$$

The material removal model can be expressed as:

$$H(y) = = \frac{k}{v_f} \cdot \int_0^{\sqrt{R^2 - y^2} - R + L} \left\{ K \times \left[\frac{x}{\tan\theta} + \frac{A\sin(2\pi f \frac{x}{v_f} + \varphi)}{\cos\theta} \right] \right\} \sqrt{\omega^2 \left[y^2 + \left(R_t - L - x \right)^2 \right] + v_f{}^2 + 2\omega \sqrt{y^2 + \left(R_t - L - x \right)^2} \cdot v_f \cdot \frac{y}{\sqrt{x^2 + y^2}}} dx \tag{22}$$

3 Polishing experiments

3.1 Experimental workpiece and experimental equipment

The experimental workpiece is a 50cm*50cm*5cm BK7 optical glass. Before experimenting, the workpiece was placed in an ultrasonic cleaner with alcohol for 10 min to ensure the cleanliness of the workpiece.

The polishing experiment was performed on the five-axis CNC polishing machine tool. The specific parameters of the polishing machine tool can be found in the previous research [29]. Different from the previous studies, a dynamometer was used to measure the polishing force during the experiments in this paper. The specific machine structure is shown in Fig. 7.

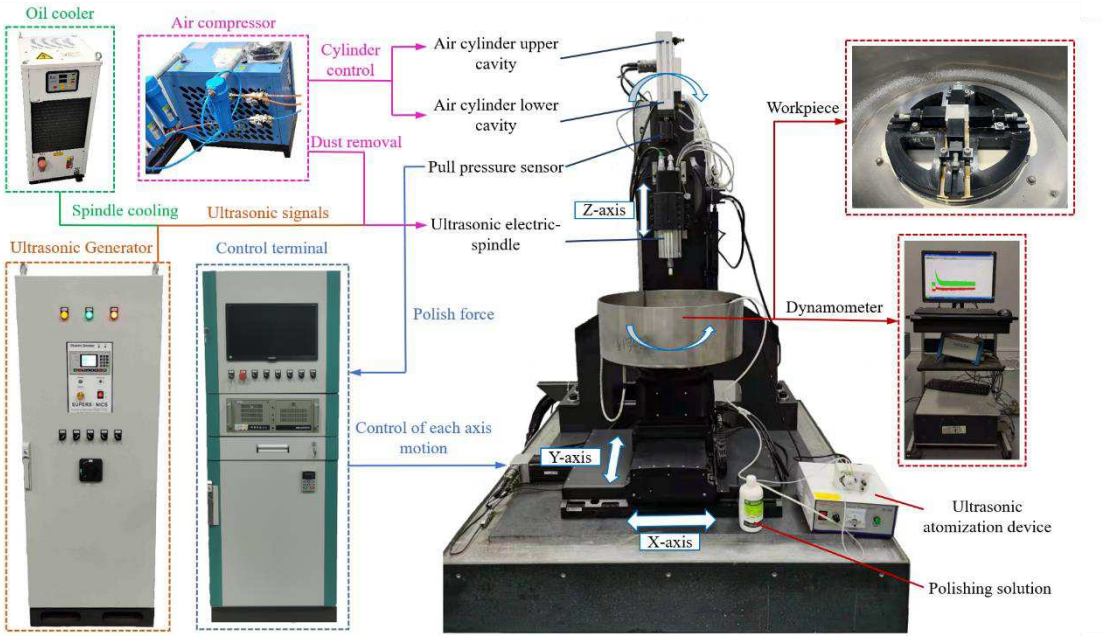

Fig. 7 Five-axis polishing machine tool

3.2 Determination of experimental parameters

The Preston coefficients in this paper were determined by pre-experiment prior to each group of experiments. By substituting Eq. (7) and Eq. (13) into Eq. (1):

$$dh(x,y)=k\omega\sqrt{x^2+\left(R_t-L-y\right)^2}\,p(t)dt \tag{23}$$

Assuming that the total polishing time is T_d, the material removal function can be given as:

$$H(x,y)=k\omega\sqrt{x^2+\left(R_t-L-y\right)^2}\int_0^{T_d}p(t)dt \tag{24}$$

In a further derivation of Eq. (24), taking the contact zone as the integration zone，the following formula can be obtained:

$$\iint H(x,y)dxdy=k\omega KLT_d\iint\sqrt{x^2+\left(R_t-L-y\right)^2}\,dxdy \tag{25}$$

In Eq. (25), volume V can be used to represent $\iint H(x,y)dxdy$, then the Preston coefficient k can be denoted as:

$$k=\frac{V}{\omega KLT_d\iint\sqrt{x^2+\left(R_t-L-y\right)^2}\,dxdy} \tag{26}$$

To ensure the accuracy of the measured Preston coefficients, the removal volumes used in this paper were obtained by 3D laser microscopy measurements. To verify the correctness of the material removal model established in this study, a series of polishing experiments were performed. The experiments variables and parameters were selected as shown in Table 1.

Table 1 Experimental parameter settings

Parameter	Value
Amplitude of ultrasonic generator (μm)	0-9
Polishing tool compression amount (mm)	0.2-0.5
Spindle speed (rpm)	6000-12000
Oblique angle of polishing-tool (°)	5-20
Feed rate of polishing tool (mm/s)	0.015
Polishing-tool dimension (mm)	10
Frequency of ultrasonic generator (Hz)	25000

4. Analysis of experiments results

The experiments workpieces were examined with a 3D laser electron microscope. The measurement results will be compared with the prediction model in four aspects: MRP, MRR, maximum removal depth and surface roughness (SR). The specific measurement results are shown in Table 2.

Table 2 Predicted and experimentally values

No.	Amplitude (μm)	Compression Volume (mm)	Rotational Speed (rpm)	Inclination Angle (°)	Maximum removal depth (μm)		Error (%)	MRR ($\times 10^{-3} \times$ mm^3/min)		Error (%)	Surface roughness (nm)
					Calculated	Measured		Calculated	Measured		
1	0	0.2	6	5	40.70	41.49	1.93	2.736	2.512	8.20	38
2	0	0.4	8	10	26.07	26.32	0.96	1.766	1.871	5.94	51
3	0	0.3	10	15	28.49	28.70	0.73	1.391	1.402	0.76	53
4	0	0.5	12	20	33.02	34.42	4.23	0.949	1.002	5.63	50
5	3	0.2	8	15	40.01	40.62	1.52	1.602	1.422	11.25	45
6	3	0.4	6	20	36.87	38.95	5.63	1.833	1.652	9.87	78
7	3	0.3	12	5	10.62	11.25	5.87	0.748	0.831	11.12	56
8	3	0.5	10	10	15.04	15.30	1.73	0.924	1.031	11.58	47
9	6	0.2	10	20	27.64	26.53	4.03	0.978	0.956	2.29	70
10	6	0.4	12	15	43.52	43.69	0.38	2.079	1.918	7.76	82
11	6	0.3	6	10	34.01	34.99	2.88	1.999	1.737	13.12	72
12	6	0.5	8	5	14.47	14.54	0.52	1.021	1.048	2.61	53
13	9	0.2	12	10	39.71	39.40	0.78	1.915	1.978	3.29	54
14	9	0.4	10	5	19.04	20.80	9.24	1.437	1.415	1.53	46
15	9	0.3	8	20	37.22	37.67	1.21	1.447	1.294	10.56	58
16	9	0.5	6	15	40.61	42.92	5.71	1.947	1.696	12.91	85

4.1 MRP analysis

Fig. 8 (a) - (p) shows the results of experiments measured MRP compared with the predicted profiles. The comparison chart shows that the material removal model developed in this paper can accurately predict the polishing profile. To evaluate the prediction effect more intuitively, the Fréchet Distance of the simulated and experimental profile curves was calculated, and the results are shown in Table 3. However, certain evaluation criteria are missing when using Fréchet Distance as the evaluation index, so the determination coefficients of the two curves were calculated in this paper using linear interpolation and linear fitting methods. According to the calculated results, the determination coefficient of both simulated and experimental removal profile curves can reach above 0.9, which proves that the two curves are well fitted. Combined with the above analysis, the prediction model can accurately predict the MRP for tilted UVAP of columnar polishing tools.

Table 3 Fréchet Distance and R^2 values

No.	1	2	3	4
Fréchet Distance	5.0254	3.0076	3.0143	3.026
R^2	0.9314	0.9586	0.9385	0.9349
No.	5	6	7	8
Fréchet Distance	3.0861	3.0065	3.3123	3.0155
R^2	0.9739	0.9086	0.9521	0.9117
No.	9	10	11	12
Fréchet Distance	3.7212	3.5772	4.0664	3.8567
R^2	0.9782	0.9174	0.927	0.9411
No.	13	14	15	16
Fréchet Distance	5.1593	2.5287	5.0004	3.24
R^2	0.9892	0.9892	0.9451	0.9251

In the experiments, it was found that the feeding direction and rotation direction

of the polishing tool would have a significant impact on the utilization rate of the polishing solution. Reasonable choice of feed direction and rotation direction can effectively prevent polishing solution splash. During the polishing process, the impact of the abrasive grains in the polishing solution on the surface of the workpiece can have a significant impact on the material removal. The splashing of the polishing solution reduces the number of effective abrasive grains, which is one of the main reasons for the difference between the theoretical model and the actual situation. In addition, machining errors and deformation of polishing tools are also important factors that lead to errors in the prediction model.

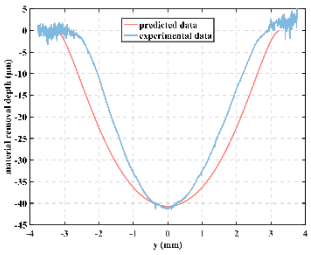

(a)

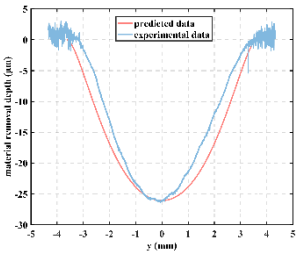

(b)

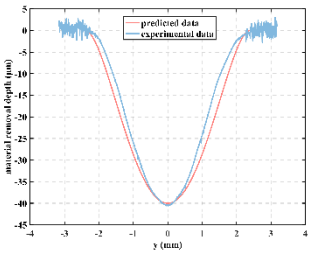

(c)

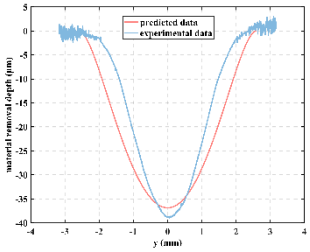

(d)

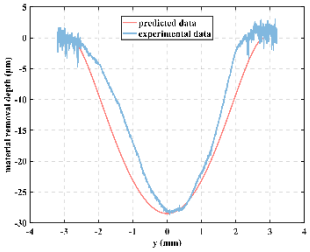

(e)

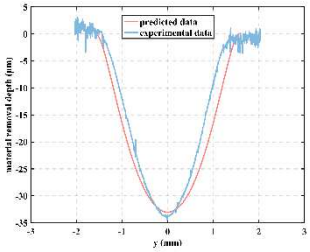

(f)

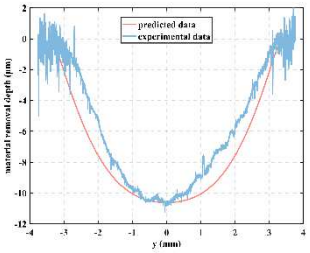

(g)

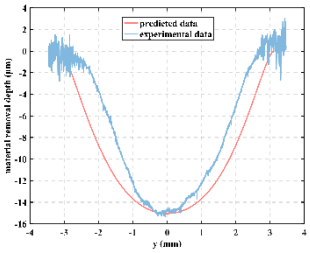

(h)

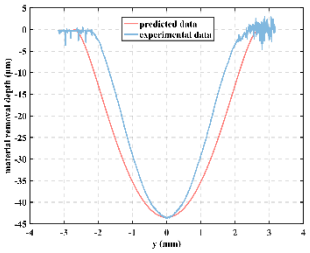

(i)

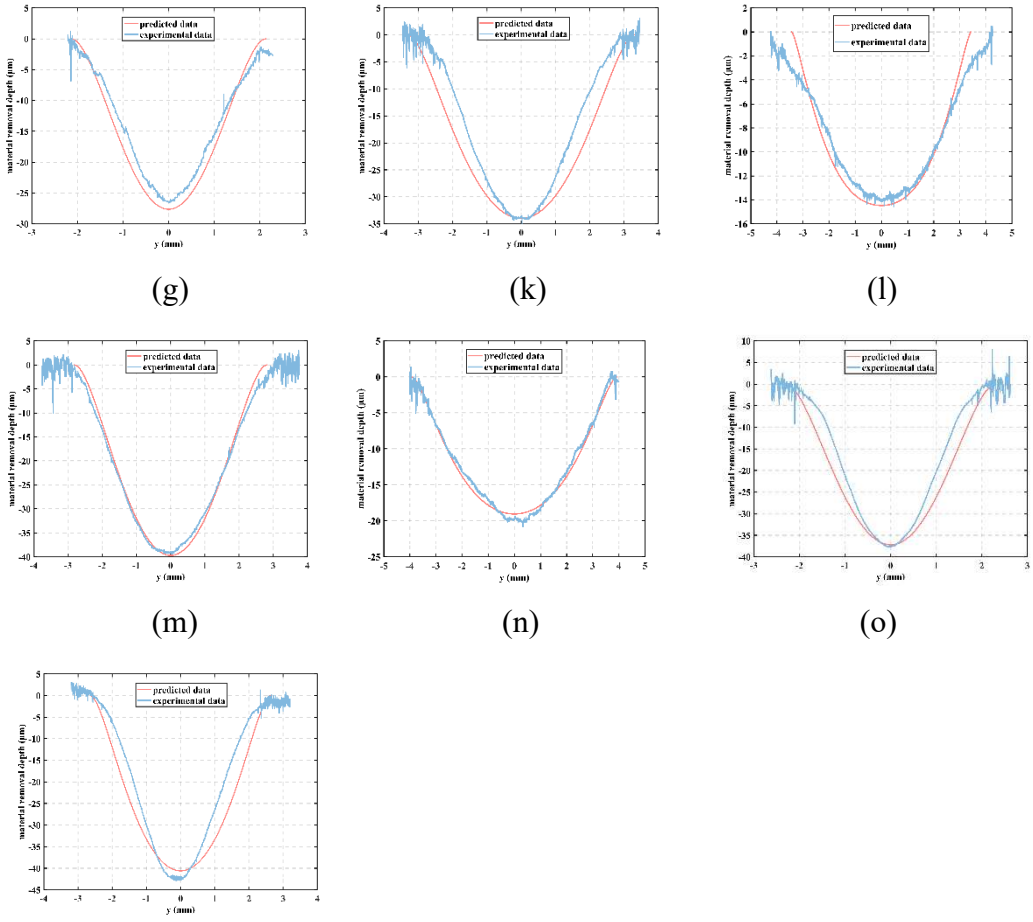

(g) (k) (l)

(m) (n) (o)

(p)

Fig. 8 Comparison between the predicted and experimental results

4.2 MRR analysis

According to the experimental data in Table 2 and Fig. 9, it can be found that the MRR errors of simulations and experiments range from 0.76% to 13.12%. The maximum error is for the 11th experimental group; the minimum error is for the 3rd experimental group. The prediction model is in better agreement with the actual processing. The experimental MRR was used as response data for ANOVA of the experimental results. The mean response table and main effects plot are shown in Table 4 and Fig. 10, respectively. The results of the analysis showed that the four variables of the experiment affected the MRR in the order of the rotational speed, compression volume, ultrasonic amplitude and inclination angle. To improve the processing

efficiency, the polishing process should maximize the MRR, so the optimal level is reached when the speed is 6000 rpm, the compression is 0.2 mm, the amplitude is 0 μm, and the tilt angle is 10°.

Table 4 Response Table for Means (MRR)

Level	Amplitude	Compression Volume	Rotational Speed	Inclination Angle
1	1.697	1.717	1.899	1.452
2	1.234	1.714	1.409	1.654
3	1.415	1.316	1.201	1.609
4	1.596	1.194	1.432	1.226
Delta	0.463	0.523	0.698	0.428
Rank	3	2	1	4

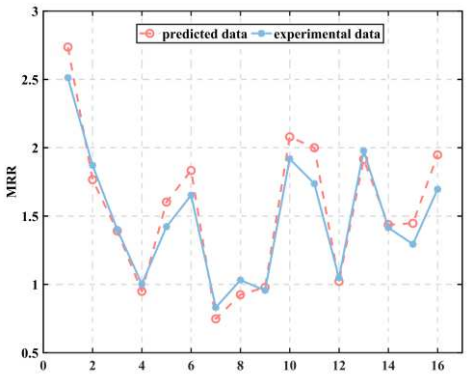

Fig. 9 MRR data comparison chart

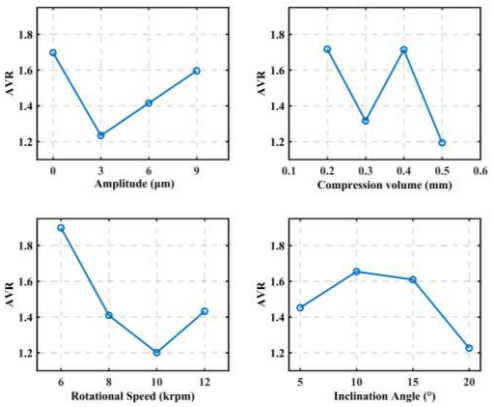

Fig. 10 Main Effects Plot for Means (MRR)

4.3 Maximum removal depth analysis

According to the experimental data in Table 2 and Fig. 11, it can be found that the errors between the predicted and experimental values range from 0.38% to 9.24%. The largest error was found in group 14; the smallest error was found in group 10. The prediction model is in better agreement with the actual situation. The experimental results were analyzed by ANOVA using the experimental maximum depth of removal as response data. The mean response table and main effects plot are shown in Table 5

and Fig. 12, respectively. The results of the analysis showed that the four variables of the experiment influenced the maximum removal depth in the order of inclination angle, rotational speed, compression volume and ultrasonic amplitude. The optimum level for maximum removal depth is when the inclination angle is 15°, the speed is 6000 rpm, the compression is 0.2 mm and the amplitude is 9 μm.

Table 5 Response Table for Means (Maximum removal depth)

Level	Amplitude	Compression Volume	Rotational Speed	Inclination Angle
1	32.73	37.01	39.59	22.02
2	26.53	32.44	29.79	29.00
3	29.94	28.15	22.83	38.98
4	35.20	26.80	32.19	34.39
Delta	8.67	10.21	16.75	16.96
Rank	4	3	2	1

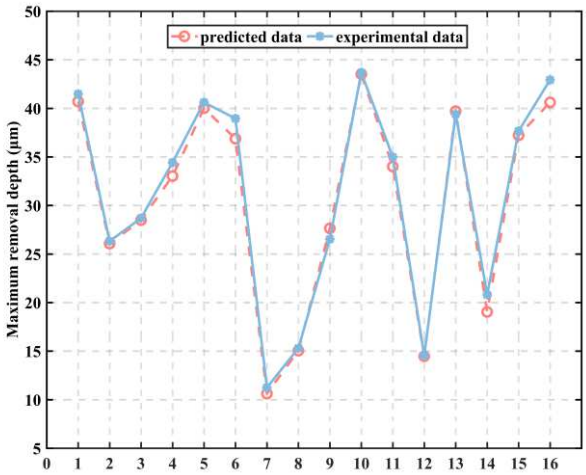

Fig. 11 Maximum removal depth analysis data comparison chart

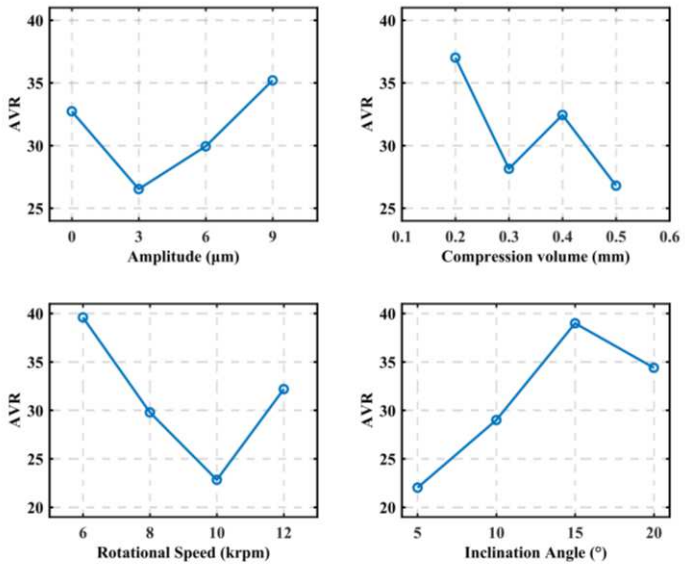

Fig. 12 Main Effects Plot for Means (Maximum removal depth)

4.4 Surface roughness (SR) analysis

According to the experimental data in Table 2, it can be found that the SR of the polished workpiece is 38 nm - 85 nm. ANOVA was performed on the experimental results using the SR of the machined workpiece as response data. The mean response table is shown in Table 6, and the SR main effects plot is shown in Fig. 13. The analysis results show that the four variables in the experiment affect the SR of the machined workpiece in the order of ultrasonic amplitude, inclination angle, rotational speed and compression. Considering the need to reduce the SR of the workpiece, the optimum level is reached when the amplitude is 0 μm, the inclination angle is 5°, the speed is 8000 rpm and the compression is 0.2 mm. Fig. 14 is a schematic diagram of part of the measurement area.

Table 6 Response Table for Means (Surface roughness)

Level	Amplitude	Compression Volume	Rotational Speed	Inclination Angle
1	48.00	51.75	68.25	48.25
2	56.50	64.25	51.75	56.00

3	69.25	59.75	54.00	66.25
4	60.75	58.75	60.50	64.00
Delta	21.25	12.50	16.50	18.00
Rank	1	4	3	2

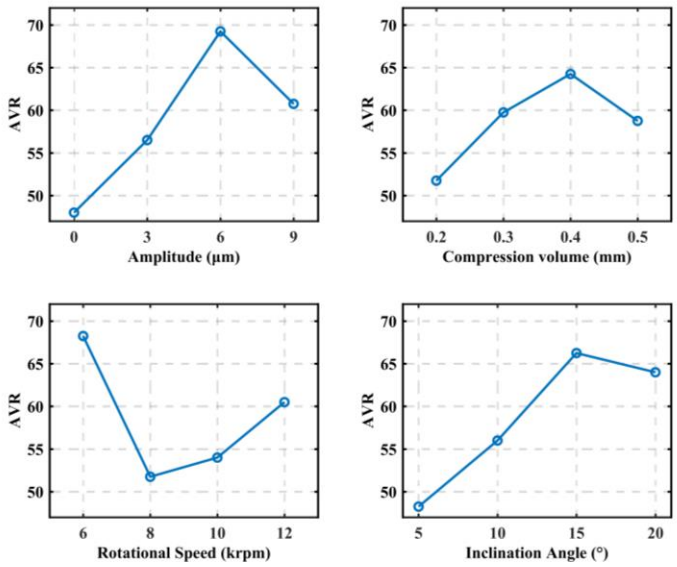

Fig. 13 Main Effects Plot for Means (Surface roughness)

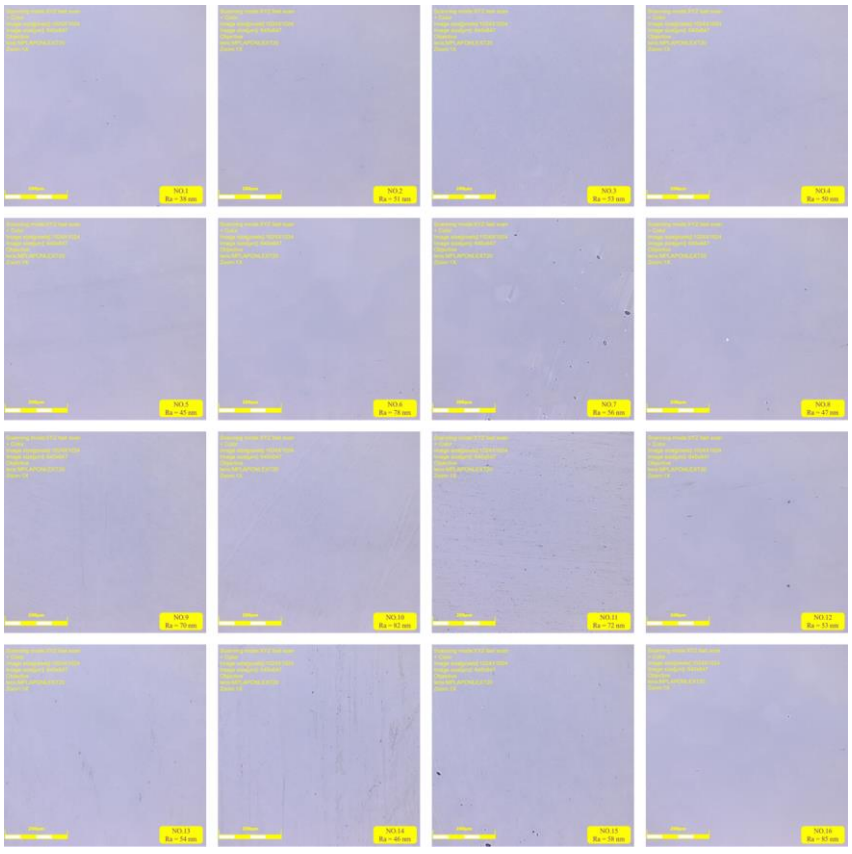

Fig. 14 Image of part of the measurement area

4.5 PSD analysis

In order to further investigate the surface condition after polishing, the polished surface was analyzed with the original surface for power spectral density (PSD) analysis, and the results of the analysis are shown in Fig. 15. The results of the original surface PSD analysis are shown in the red curve in this figure. The analysis results show that ultrasonic vibration-assisted polishing can have an effective reduction of medium and high frequency errors, and has an extremely significant effect on reducing high frequency errors.

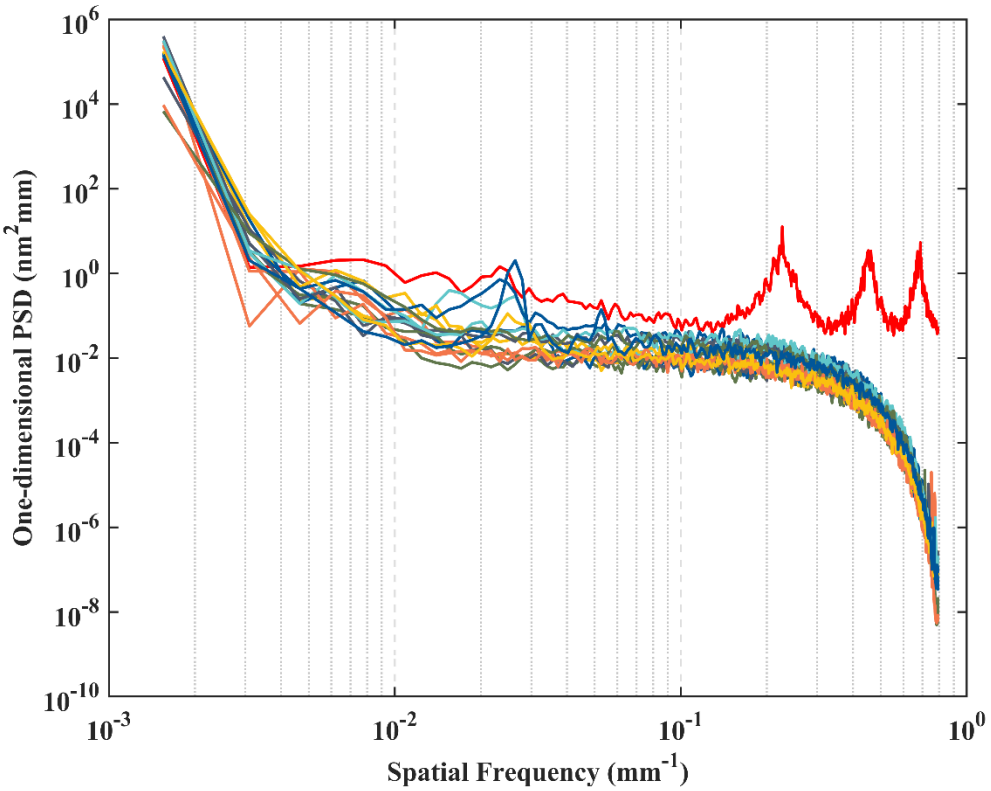

Fig. 15 PSD comparison analysis of machined surface and original surface

To further investigate the surface evolution mechanism during UVAP, BK7 glass was polished using different ultrasonic amplitudes, respectively, and the results of the PSD analysis are shown in Fig. 16. It can be found that when the frequency is low (frequency is less than the position of X point marked in this figure) ultrasonic vibration

has less effect on the spatial frequency error; with the increase of spatial frequency, ultrasonic vibration plays a certain effect on reducing the error. With the increase of ultrasonic amplitude, the spatial frequency error has a tendency to gradually decrease. Therefore, ultrasonic vibration-assisted polishing can reduce the high-frequency error in the processed workpiece surface and help improve the optical properties of processed BK7 glass, and the processing effect will become better with the increase of amplitude.

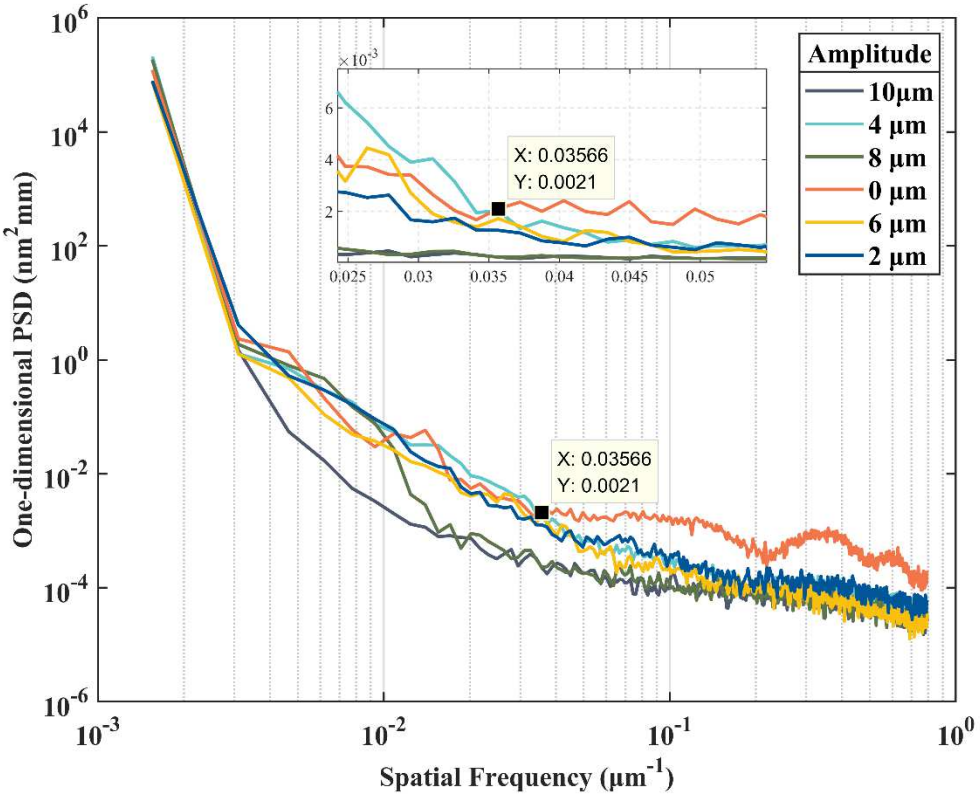

Fig. 16 Comparative analysis of PSD on machined surfaces with different amplitudes

5. Conclusion

1. An effective UVAP model of material removal for a tilted column polishing tool was developed. The distribution model of polishing pressure within the contact zone was determined by normal loading tests on BK7 glass. The distribution of linear

velocity within the contact zone was also investigated using geometric analysis. Compared with previous material removal models, this model takes into account the effect of ultrasonic vibrations.

2. A series of experiments were conducted to verify the reliability of the prediction model from several aspects. The experimental results showed that the coefficient of determination between the predicted curve and the actual removal profile was above 0.9. The MRR error values ranged from 0.76% to 13.12%, and most of the error values were below 10%. The maximum removal depth error values are in the range of 0.37% - 9.24%. The surface roughness of the machined workpiece is 38nm - 85nm.

3. The ANOVA was performed based on the results of an orthogonal test. It shows that the four variables chosen in the experiment influence the MRR in the order of rotational speed, compression volume, ultrasonic amplitude and inclination angle. The degree of influence on the maximum removal depth was in the order of inclination angle, rotational speed, compression volume and amplitude. The degree of influence on the SR of the machined workpiece was determined in the order of amplitude, inclination angle, rotational speed and compression volume. And the optimal level of each factor was determined.

4. PSD analysis of the experimental results was conducted. The analysis results show that UVAP can effectively reduce the medium frequency and high frequency errors on the processed workpiece surface. And the processing effect gradually improves with the increase of ultrasonic amplitude.

Based on the above, this paper establishes a UVAP model of material removal for

tilted column polishing tools, which can effectively predict the surface profile after UVAP processing. It is a good guide to achieving material deterministic removal by UVAP. In future work, curved surfaces will be studied as objects for more in-depth material removal models.

Funding

This work was supported by the Major State Basic Research Development Program of China [Grant No. 2017YFA0701200]; the National Natural Science Foundation of China [Grant No. 52075088]; the Northeastern University Postdoctoral Foundation [Grant No.20210309].

Conflicts of interest

The authors declare no competing interests.

Data Availability

The datasets supporting the conclusion of this article are included within the article.

Code Availability

Not applicable.

Ethics approval

Not applicable.

Consent to participate

The authors agree to the authorship order.

Consent for publication

All authors have read and agreed to the published version of the manuscript.

Authors' contributions

Zhijie Cui: Conceptualization, Methodology, Software, Investigation, Experiment, Writing - original draft, Writing - review & editing. **Yingdong Liang:** Experiment, Writing - review & editing. **Xin Chen:** Experiment, Writing - review & editing. **Fanwei Meng:** Experiment, Formal analysis. **Zixuan Wang:** Funding acquisition. Writing - review & editing. **Tianbiao Yu:** Resources, Supervision, Writing - review & editing. Funding acquisition. **Ji Zhao:** Resources, Supervision, Funding acquisition.

References

1. Qu S, Yao P, Gong Y, et al (2022) Modelling and grinding characteristics of unidirectional C–SiCs. Ceram Int 48:8314–8324. https://doi.org/10.1016/j.ceramint.2021.12.036
2. Sui M, Li C, Wu W, et al (2021) Temperature of Grinding Carbide with Castor Oil-Based MoS2 Nanofluid Minimum Quantity Lubrication. J Therm Sci Eng Appl 13:. https://doi.org/10.1115/1.4049982
3. Ma Z, Wang Q, Chen H, et al (2022) A grinding force predictive model and experimental validation for the laser-assisted grinding (LAG) process of zirconia ceramic. J Mater Process Technol 302:117492. https://doi.org/10.1016/j.jmatprotec.2022.117492
4. Feng J, Huang X, Yang S, et al (2021) Speed effect on the material behavior in high-speed scratching of BK7 glass. Ceram Int 47:19978–19988.

https://doi.org/10.1016/j.ceramint.2021.04.008
5. Zhang Y, Yan G, You K, Fang F (2020) Study on α-Al2O3 anti-adhesion coating for molds in precision glass molding. Surf Coatings Technol 391:125720. https://doi.org/10.1016/j.surfcoat.2020.125720
6. Melentiev R, Fang F (2021) Prediction of crater depth, surface roughness and erosion rate during abrasive jet machining of glass. Wear 468–469:203596. https://doi.org/10.1016/j.wear.2020.203596
7. Gu W, Yao Z, Liang X (2011) Material removal of optical glass BK7 during single and double scratch tests. Wear 270:241–246. https://doi.org/10.1016/j.wear.2010.10.064
8. Pal RK, Garg H, Sarepaka RG V., Karar V (2016) Experimental Investigation of Material Removal and Surface Roughness during Optical Glass Polishing. Mater Manuf Process 31:1613–1620. https://doi.org/10.1080/10426914.2015.1103867
9. Kumar S, Singh AK (2018) Magnetorheological nanofinishing of BK7 glass for lens manufacturing. Mater Manuf Process 33:1188–1196. https://doi.org/10.1080/10426914.2017.1364759
10. Lv D, Huang Y, Tang Y, Wang H (2013) Relationship between subsurface damage and surface roughness of glass BK7 in rotary ultrasonic machining and conventional grinding processes. Int J Adv Manuf Technol 67:613–622. https://doi.org/10.1007/s00170-012-4509-1
11. Pal RK, Sharma R, Baghel PK, et al (2018) An approach for quantification of friction and enhancing the process efficiency during polishing of optical glass. J Mech Sci Technol 32:3835–3842. https://doi.org/10.1007/s12206-018-0735-2
12. Huang C, Zhou M, Zhang H (2021) A cutting force prediction model in axial ultrasonic vibration end grinding for BK7 optical glass considering protrusion height of abrasive grits. Meas J Int Meas Confed 180:109512. https://doi.org/10.1016/j.measurement.2021.109512
13. Zhao PY, Zhou M, Liu XL, Jiang B (2020) Effect to the surface composition in ultrasonic vibration-assisted grinding of BK7 optical glass. Appl Sci 10:. https://doi.org/10.3390/app10020516
14. Yang M, Li C, Luo L, et al (2021) Predictive model of convective heat transfer coefficient in bone micro-grinding using nanofluid aerosol cooling. Int Commun Heat Mass Transf 125:105317. https://doi.org/10.1016/j.icheatmasstransfer.2021.105317
15. Yang M, Li C, Zhang Y, et al (2019) Effect of friction coefficient on chip thickness models in ductile-regime grinding of zirconia ceramics. Int J Adv Manuf Technol 102:2617–2632. https://doi.org/10.1007/s00170-019-03367-0
16. Yang M, Li C, Said Z, et al (2021) Semiempirical heat flux model of hard-brittle bone material in ductile microgrinding. J Manuf Process 71:501–514. https://doi.org/10.1016/j.jmapro.2021.09.053
17. Guo X, Zhai R, Shi Y, et al (2020) Study on influence of grinding depth and grain shape on grinding damage of K9 glass by SPH simulation. Int J Adv Manuf Technol 106:333–343. https://doi.org/10.1007/s00170-019-04649-3
18. Zhang Y, Fang F, Huang W, Fan W (2021) Dwell Time Algorithm Based on

Bounded Constrained Least Squares Under Dynamic Performance Constraints of Machine Tool in Deterministic Optical Finishing. Int J Precis Eng Manuf - Green Technol 8:1415–1427. https://doi.org/10.1007/s40684-020-00306-3
19. Guo X, Huang J, Yuan S, et al (2021) Study using ReaxFF-MD on the CMP process of fused glass in pure H2O/aqueous H2O2. Appl Surf Sci 556:149756. https://doi.org/10.1016/j.apsusc.2021.149756
20. Wang K, Yan Y, Zhou P, et al (2020) Preparation of Flat and Smooth Copper Surface by Jet Electrochemical Machining and Electrochemical Polishing. J Electrochem Soc 167:163501. https://doi.org/10.1149/1945-7111/abcbb2
21. Zhang C, Qu S, Liang Y, et al (2022) Predictive modeling and experimental study of polishing force for ultrasonic vibration-assisted polishing of K9 optical glass. Int J Adv Manuf Technol 119:3119–3139. https://doi.org/10.1007/s00170-021-08624-9
22. Liang Y, Zhang C, Chen X, et al (2022) Modeling and analysis of the material removal rate for ultrasonic vibration–assisted polishing of optical glass BK7. Int J Adv Manuf Technol 118:627–639. https://doi.org/10.1007/s00170-021-07967-7
23. Kang D, Zou P, Wu H, et al (2020) Theoretical and experimental study of ultrasonic vibration-assisted laser polishing 304 stainless steel. IEEE Access 8:206146–206163. https://doi.org/10.1109/ACCESS.2020.3036403
24. Qu S, Wang Z, Zhang C, et al (2021) Material removal profile prediction and experimental validation for obliquely axial ultrasonic vibration-assisted polishing of K9 optical glass. Ceram Int 47:33106–33119. https://doi.org/10.1016/j.ceramint.2021.08.212
25. Xiao MB, Ding Y, Fang Z, Yang G (2020) Contact force modeling and analysis for robotic tilted-disc polishing of freeform workpieces. Precis Eng 66:188–200. https://doi.org/10.1016/j.precisioneng.2020.04.019
26. Wang QH, Liang YJ, Xu CY, et al (2019) Generation of material removal map for freeform surface polishing with tilted polishing disk. Int J Adv Manuf Technol 4213–4226. https://doi.org/10.1007/s00170-019-03478-8
27. Zhang T, Guan C, Zhang C, et al (2021) Predictive modeling and experimental study of generated surface-profile for ultrasonic vibration-assisted polishing of optical glass BK7 in straight feeding process. Ceram Int 47:19809–19823. https://doi.org/10.1016/j.ceramint.2021.03.320
28. Feng D, Sun Y, Du H (2014) Investigations on the automatic precision polishing of curved surfaces using a five-axis machining centre. Int J Adv Manuf Technol 72:1625–1637. https://doi.org/10.1007/s00170-014-5774-y
29. Cui Z, Meng F, Liang Y, et al (2022) Sub-regional polishing and machining trajectory selection of complex surface based on K9 optical glass. J Mater Process Technol 304:117563. https://doi.org/10.1016/j.jmatprotec.2022.117563